Earth and Planetary Science Letters ••• (••••) •••–•••

Contents lists available at ScienceDirect

Earth and Planetary Science Letters

www.elsevier.com/locate/epsl

Regional changes in streamflow after a megathrust earthquake

Christian H. Mohr [a,*], Michael Manga [b], Chi-Yuen Wang [b], Oliver Korup [a]

[a] Institute of Earth and Environmental Sciences, University of Potsdam, Karl-Liebknecht-Strasse 24–25, D-14476 Potsdam, Germany
[b] Department of Earth and Planetary Science, University of California, 307 McCone Hall, Berkeley, CA 94720, USA

ARTICLE INFO

Article history:
Received 10 August 2016
Received in revised form 2 November 2016
Accepted 6 November 2016
Available online xxxx
Editor: P. Shearer

Keywords:
Maule earthquake
streamflow response
permeability
groundwater flow modeling
earthquake hydrology

ABSTRACT

Moderate to large earthquakes can increase the amount of water feeding stream flows, mobilizing excess water from deep groundwater, shallow groundwater, or the vadose zone. Here we examine the regional pattern of streamflow response to the Maule M8.8 earthquake across Chile's diverse topographic and hydro-climatic gradients. We combine streamflow analyses with groundwater flow modeling and a random forest classifier, and find that, after the earthquake, at least 85 streams had a change in flow. Discharge mostly increased ($n = 78$) shortly after the earthquake, liberating an excess water volume of >1.1 km^3, which is the largest ever reported following an earthquake. Several catchments had increased discharge of >50 mm, locally exceeding seasonal streamflow discharge under undisturbed conditions. Our modeling results favor enhanced vertical permeability induced by dynamic strain as the most probable process explaining the observed changes at the regional scale. Supporting this interpretation, our random forest classification identifies peak ground velocity and elevation extremes as most important for predicting streamflow response. Given the mean recurrence interval of ~25 yr for >M8.0 earthquakes along the Peru–Chile Trench, our observations highlight the role of earthquakes in the regional water cycle, especially in arid environments.

© 2016 Elsevier B.V. All rights reserved.

1. Introduction

Hydrological changes after earthquakes have been documented for millennia (e.g., Pliny, ca. AD 77–79), including changing water levels in wells, liquefaction of soils, altered activity of mud volcanoes and geysers, and the formation and disappearance of springs (Muir-Wood and King, 1993; Rojstaczer et al., 1995; Wang and Manga, 2010a). Streamflow responses include co- and post-seismic increases (Montgomery et al., 2003), decreases (Wang et al., 2004a), or both (Mohr et al., 2012), as earthquakes change crustal stresses, hydraulic heads, and physical properties such as the permeability of the subsurface, all controlling water flux. Altered stream discharge following earthquakes have been observed in the near- and intermediate field (Rojstaczer et al., 1995). The near field is defined as the area within one fault length of the rupture, whereas the intermediate field enfolds an area within several fault lengths. Seismically triggered streamflow changes are more than curiosities, and provide rare opportunities to study the water cycle under pulsed disturbances. Hence, earthquakes may provide important insights into the regional hydrological cycle and near-surface hydro-seismological processes that are difficult, if not impossible, to study otherwise. Understanding earthquake hydrology may reveal details about hydrocarbon migration (Beresnev and Johnson, 1994), the dynamics of geothermal systems (Manga et al., 2012), the security of water supplies (Chen and Wang, 2009), the integrity of waste repositories (Carrigan et al., 1991), and biological activity, such as modified invertebrate fauna in streams affected by post-seismic changes in streamflow and hydrochemistry (Galassi et al., 2014).

Earthquakes cause static and dynamic strain, which directly affect streamflow via increases in pore pressure caused by static strain (Muir-Wood and King, 1993), consolidation (up to liquefaction) by dynamic strain (Manga, 2001; Montgomery et al., 2003), increased permeability (Rojstaczer et al., 1995; Wang et al., 2004a), or the release of vadose zone water by dynamic strain (Manga and Rowland, 2009; Mohr et al., 2015). Each of these mechanisms is physically plausible and might explain the observed streamflow responses, though detailed studies have drawn conflicting conclusions about the dominant mechanism. For example, the isotopic composition of excess water emerging in previously dry streams pointed to a groundwater source after the 2014 Mw6.0 South Napa earthquake (Wang and Manga, 2015). In contrast, modeling for headwater streams in south-central Chile, an area that is comparable to northern California in terms of its hydro-climatic conditions, indicated that water was shaken out of the vadose

* Corresponding author. Fax: +49 331 977 2068.
E-mail addresses: cmohr@uni-potsdam.de (C.H. Mohr), manga@seismo.berkeley.edu (M. Manga), chiyuen@berkeley.edu (C.-Y. Wang), oliver.korup@geo.uni-potdam.de (O. Korup).

http://dx.doi.org/10.1016/j.epsl.2016.11.013
0012-821X/© 2016 Elsevier B.V. All rights reserved.

zone after the 2010 Maule M8.8 earthquake (Mohr et al., 2015). The hypothesis that strong ground shaking enhances permeability (Rojstaczer et al., 1995; Wang et al., 2004a) is consistent with lowered water temperatures (Wang et al., 2012) and altered electrical conductivity (Charmoille et al., 2005), but incompatible with unchanged recession constants after earthquakes (Manga, 2001; Montgomery et al., 2003). Recession constants are widely used to describe the hydraulic permeability at the catchment scale (Blume et al., 2007). Groundwater flow is governed by Darcy's law, so if permeability does not change, the hydraulic head has to increase instead. Accordingly, Manga (2001) and Montgomery et al. (2003) proposed that coseismic consolidation of saturated deposits increased the hydraulic head. Another hypothesis is that the vertical permeability was enhanced by earthquakes, which increased the base flow feeding streams (Fleeger and Goode, 1999; Wang et al., 2004a, 2004b; Wang and Manga, 2015).

Why do catchments respond in such different ways to earthquakes even under comparable environmental conditions? What are the underlying controls? Guided by these research questions, our objectives are (a) to identify regional patterns in streamflow responses to the M8.8 2010 Maule earthquake, Chile, (b) to identify environmental controls on the observed streamflow anomalies, and (c) to reconcile these anomalies with a groundwater flow model. To this end, we combine random forest classification of potential predictors of streamflow changes with physics-based 1D-groundwater modeling for catchments showing altered discharges following the Maule earthquake.

2. Study area, data and methods

2.1. Study area

Chile is well suited for studying earthquake hydrology because of the country's distinct environmental contrasts. With some of the driest and wettest spots on Earth, Chile has a steep hydro-climatic gradient. Mean annual rainfall varies between less than 10 mm and more than 2000 mm (Hijmans et al., 2005), and potential evapotranspiration varies by more than an order of magnitude (Fig. 1). The trade-off between water supply and demand determines the effective aridity. Chile hosts some of the world's steepest topographic gradients, and the Andes reach ~7000 m asl, while the Coastal Mountain ranges are >3000 m asl in the north (Fig. 1). The country is also prone to frequent earthquake shaking. According to the ANSS earthquake catalogue (NCEDC, 2014), Chile has experienced >M8.0 earthquakes every 25 yr on average (Fig. 2).

2.2. Data

We examined time series of daily averaged discharge at 716 stream gauging stations, rainfall at 802 precipitation gauges, and air temperature at 75 meteorological stations, provided by the Dirección General de Aguas (DGA) (http://dgasatel.mop.cl/). The stations are spread across Chile from the Atacama Desert and Altiplano in the north to Tierra del Fuego in the south (Fig. 1), and sample headwater streams as well as larger catchments with multiple tributaries, including lowland rivers of the Central Valley.

For each catchment we compiled several attributes. We grouped the geological map of Chile (SERNAGEOMIN, 2003) into metamorphic, sedimentary, and igneous rocks, as well as unconsolidated sediments, and computed the fraction of each class within each catchment. We calculated the distance between the gauging stations and the nearest (mapped) fault, and estimated fault density (km/km^2) in each catchment. This density estimate includes all normal, reverse, and strike–slip faults mapped by SERNAGEOMIN (2003). We used annual precipitation data from the BIOCLIM data (Hijmans et al., 2005) for the period between 1950 and 2000

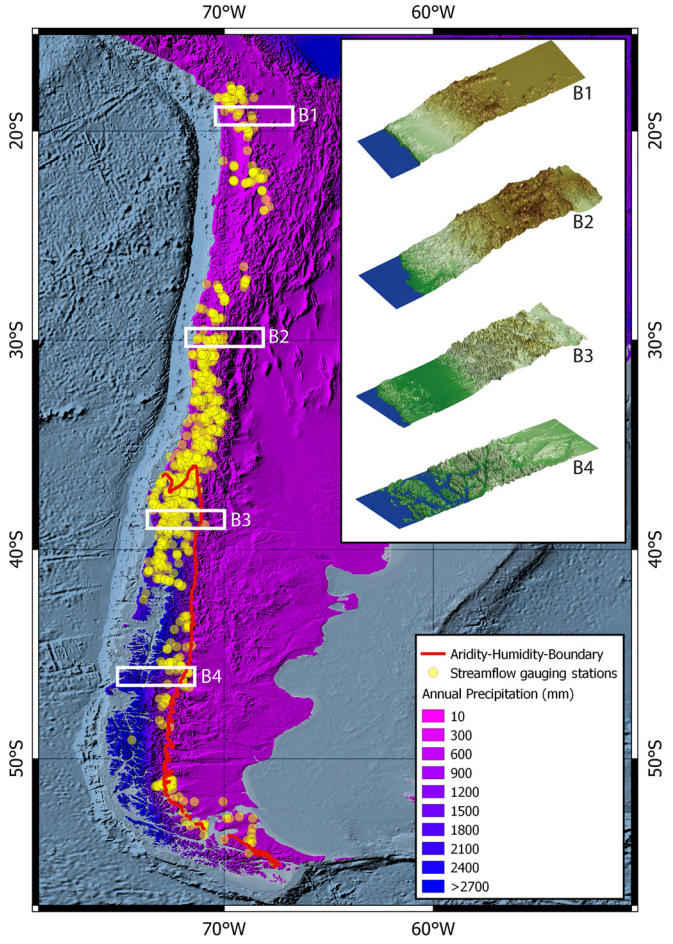

Fig. 1. Geographical setting. Average annual precipitation (mm) for the period between 1950–2000 based on BIOCLIM data (Hijmans et al., 2005) for Chile. Yellow circles show streamflow gauging stations operated by Chilean Direccion General de Aguas (DGA). Red line indicates the aridity–humidity boundary, i.e. the ratio of mean annual precipitation and mean annual potential evapotranspiration (Zorner et al., 2008). Topography is based on SRTM data (Jarvis et al., 2008), bathymetry comes from the ESRI World Ocean Baselayer. The inset shows 100-km wide topographic swath profiles based on SRTM data (Jarvis et al., 2008) to illustrate the topographic gradients across Chile. (http://services.arcgisonline.com/arcgis/rest/services/Ocean/World_Ocean_Base, accessed 05.06.2016.) (For interpretation of the references to color in this figure legend, the reader is referred to the web version of this article.)

derived from summing monthly rainfall data. We used average annual rainfall to estimate how much water entered the catchments during a hydrological year. To account for rainfall prior to the earthquake, we also included the long-term (1950–2000) averaged February precipitation, as the earthquake occurred at the end of that month. We (re)classified the land-cover information in global mosaics of the standard MODIS land-cover type data product (MCD12Q1) at 500-m resolution (Channan et al., 2014; Friedl et al., 2010), and LANDSAT images (2000–2005) at 30-m resolution (Sexton et al., 2013). We used data on peak ground acceleration (PGA) and peak ground velocity (PGV) generated by the M8.8 Maule earthquake published by the USGS (http://earthquake.usgs.gov/earthquakes/shakemap/global/shake/2010tfan/#download), and modeled static strain within each catchment using Coulomb 3.3 (Lin and Stein, 2004; Toda et al., 2005), and model parameters provided by Chen Ji (University of California, Santa Barbara, http://www.geol.ucsb.edu/faculty/ji/big_earthquakes/2010/02/27/chile_2_27.html).

Some of the published gauge locations at catchment outlets seemed questionable. We thus estimated the most plausible location requiring that the distance to the published outlet location

Please cite this article in press as: Mohr, C.H., et al. Regional changes in streamflow after a megathrust earthquake. Earth Planet. Sci. Lett. (2016), http://dx.doi.org/10.1016/j.epsl.2016.11.013

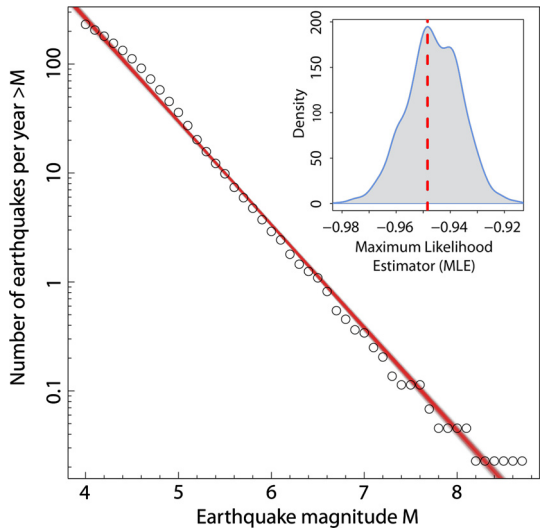

Fig. 2. Earthquake magnitude–frequency. Magnitude–frequency relationship derived for 11 533 earthquakes >M4 from ANSS data (January 1970 to December 2014) (NCEDC, 2014). Vertical axis is number of earthquakes with magnitude greater than shown on the *x*-axis. Red lines are maximum likelihood estimates from bootstrapped regression on log-binned data. Inset shows bootstrap (1000 iterations) density estimate of maximum likelihood estimator of modeled power-law slope ($b \sim -0.948$). Mode is indicated by the red dashed line. (For interpretation of the references to color in this figure legend, the reader is referred to the web version of this article.)

be minimized (within a maximum of 2 km), though agreeing as closely as possible with the published catchment area and flow path. We normalized the resulting misfits to account for differences in catchment size, and aggregated the errors into a single value describing the total misfit. Based on these recalculated locations, we adjusted catchment area and derived topographic metrics such as elevation and local slope from a 90-m SRTM digital elevation model (Jarvis et al., 2008) with TopoToolbox 2 (Schwanghart and Scherler, 2014) to broadly characterize the topography of the catchments.

We analyzed 293 streams with complete discharge data before and after the Maule earthquake, and visually classified the hydrographs into (1) post-seismic increases, (2) post-seismic decreases, and (3) no response.

We checked for effects of snow or glacial melt, which is mostly relevant for the catchments fed by high Andean headwaters during summer, by determining the maximum cross-correlation coefficient and corresponding time lag between the discharge records and the three nearest air temperature records. Assuming a temperature-driven signal in the post-seismic streamflow, we expect that both time series closely correlate with the temperature signal preceding the streamflow response due to heat exchange with the land and/or atmosphere.

We then computed the relative change in streamflow induced by the earthquake by comparing discharges before and after in the period between February 28 to March 31, 2010.

2.3. Recession analysis

Hydraulic diffusivity is closely related to the geometrical and physical properties of the aquifer. The recession constant can be used to characterize the hydraulic diffusivity. We compared pre- and post-seismic recession constants calculated by the constant *k* method (Blume et al., 2007) to explore possible seismic effects on hydraulic diffusivity:

$$\frac{\delta Q}{\delta t} = -k \cdot Q(t) \tag{1}$$

which can be rearranged to

$$k = -\frac{\delta Q}{\delta t} \cdot 1/Q(t) \tag{2}$$

where k is the recession constant (1/day) and $Q(t)$ is discharge at time t (m^3/s). Hydraulic diffusivity is not necessarily constant but may decrease with depth and, thus, change with aquifer thickness (Beven, 1995). One may thus argue that thicker aquifers have lower averaged hydraulic diffusivity. However, hydraulic diffusivity can also be regarded as locally constant (e.g., Kampf and Burges, 2007), a simplification that we adopt here even if water levels change. Assuming linear groundwater storage, baseflow recession should decline exponentially (Blume et al., 2007). In determining the recession coefficient k of the exponential function in equation (2) for pre- and post-seismic periods on the hydrograph, it is thus possible to quantify changes in diffusivity induced by the earthquake. We estimated the recession constants k for base flow for one year before and after the earthquake, separating base flow from total flow with a base flow filter (Nathan and McMahon, 1990).

2.4. Random forest classifier

We used a random forest classifier (Breiman, 2001) to identify the most important catchment- and earthquake-related controls that might determine the presence or absence of streamflow responses. Random forests are ensembles of decision trees trained on data, forming a robust nonparametric model capable of handling large nonlinear, noisy, fragmented, or correlated multidimensional data for classification (Liaw and Wiener, 2002; Strobl et al., 2008), and combine bootstrap aggregating with random variable selection (Breiman, 2001). The strategy is to explore the importance of predictors using bootstrapped data and predictor subsets for growing decision trees. In random forest, each tree node is split using the best among a subset of predictors randomly chosen at that node. This approach performs very well compared to other classifiers such as support vector machines or neural networks, and remains robust against overfitting (Breiman, 2001; Liaw and Wiener, 2002). The random forest algorithm includes three main steps:

1. Draw n bootstrap samples from the data set.
2. Grow a classification tree for each bootstrap sample, randomly sample at each split a subset of the predictors and chose the best split among them. At each split, the data are divided into two groups following a simple rule aimed at minimizing the total variance.
3. Predict new data from the majority vote of all trees' predictions.

At each bootstrap iteration, random forest predicts the data not included in the bootstrap data (so called "out-of-bag") using the tree grown on the bootstrap sample. After aggregating all out-of-bag predictions, the overall error rate is estimated (Breiman, 2001). The main parameters of random forests are the number of trees, the trees' complexity, the number of randomly selected predictor variables at each split, and the size of the training set (Breiman, 2001). The relative loss of model performance when omitting a specific predictor defines that predictor's importance, if corrected for spurious correlation effects (Strobl et al., 2008). To this end, we calculated the out-of-bag-prediction accuracy, and determined all split points for each predictor variable in a given tree. We then randomly permuted the split-point values and re-assessed the out-of-bag-prediction accuracy. The difference between pre- and post-permutation prediction accuracy provides the conditioned im-

Please cite this article in press as: Mohr, C.H., et al. Regional changes in streamflow after a megathrust earthquake. Earth Planet. Sci. Lett. (2016), http://dx.doi.org/10.1016/j.epsl.2016.11.013

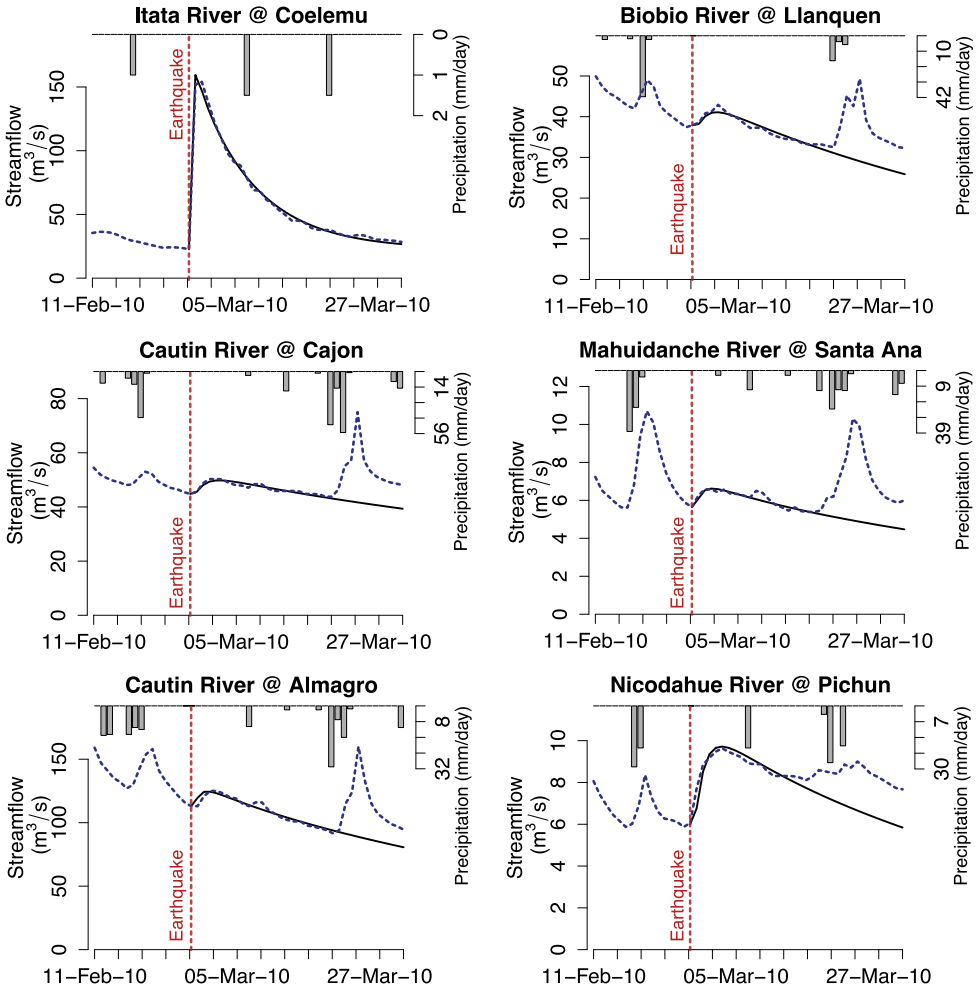

Fig. 3. Hydrographs. Sample hydrographs showing post-seismic increase in river discharge (Fig. 4 shows locations). Black curve is fit from seismically triggered groundwater flow model (m^3/s) (equation (7)); blue dashed line is measured streamflow (m^3/s); histogram shows daily precipitation data (mm/day). (For interpretation of the references to color in this figure legend, the reader is referred to the web version of this article.)

portance of each predictor for a single tree. We thus computed the overall variable importance for the random forest by averaging over all trees (Strobl et al., 2008).

Our response variable refers to the presence or absence of post-seismic streamflow responses. Predictor variables include continuous data on hydro-climatology, geology, tectonics, land cover, topography, and earthquake properties (Supplement 1). We grew random forests with 1000 individual trees, setting the number of variables at each node to 18 (out of a total of 54 predictors). Though this setup is slightly higher than the recommended number (Liaw and Wiener, 2002), the model performance was best using that number of nodes; the number of predictor variables is largely a tuning parameter (Hastie et al., 2009).

2.5. Groundwater flow modeling

One-dimensional groundwater models are popular and geometrically simplified tools for interpreting hydrological responses to earthquakes, as available observations are unable to support more complex models (Manga, 2001; Manga and Wang, 2015; Mohr et al., 2015; Rojstaczer et al., 1995; Wang and Manga, 2015, 2010a). Our key assumption is that water is released, either from the saturated or unsaturated zone, to recharge an aquifer during or in the wake of strong earthquake shaking (Wang et al., 2004a). The linearized Boussinesq equation and Darcy's equation describe groundwater flow in space x and time t for unconfined or confined aquifers, respectively:

$$\frac{\partial h}{\partial t} = D\frac{\partial^2 h}{\partial x^2} + \frac{A}{S_S}(x,t) \tag{3}$$

with

$$Q = -K * D_t * \frac{\partial h}{\partial x} \tag{4}$$

where A is the rate of water recharge per unit width of the release zone $(1/T)$, S_S is specific yield $(1/L)$, Q is the groundwater discharge exiting the aquifer (L^3/T), h is hydraulic head (L) above the background value elevated by the earthquake, K is the hydraulic conductivity (L/T), D is the hydraulic diffusivity (L^2/T), and D_t is the cross-sectional area of the aquifer (L^2). The Boussinesq model applies here, because the ratio between horizontal and vertical flow is high enough to justify horizontal flow only and, thus, $1D$ flow conditions (Guérin et al., 2014). We treat hydraulic diffusivity D as constant, and assume that streamflow was sustained from saturated flow so that Darcian flow applies. The aquifer extends from $x = 0$ at the catchment divide to $x = U$ at the channel. The boundary conditions are

$$h(U,t) = 0 \tag{5}$$

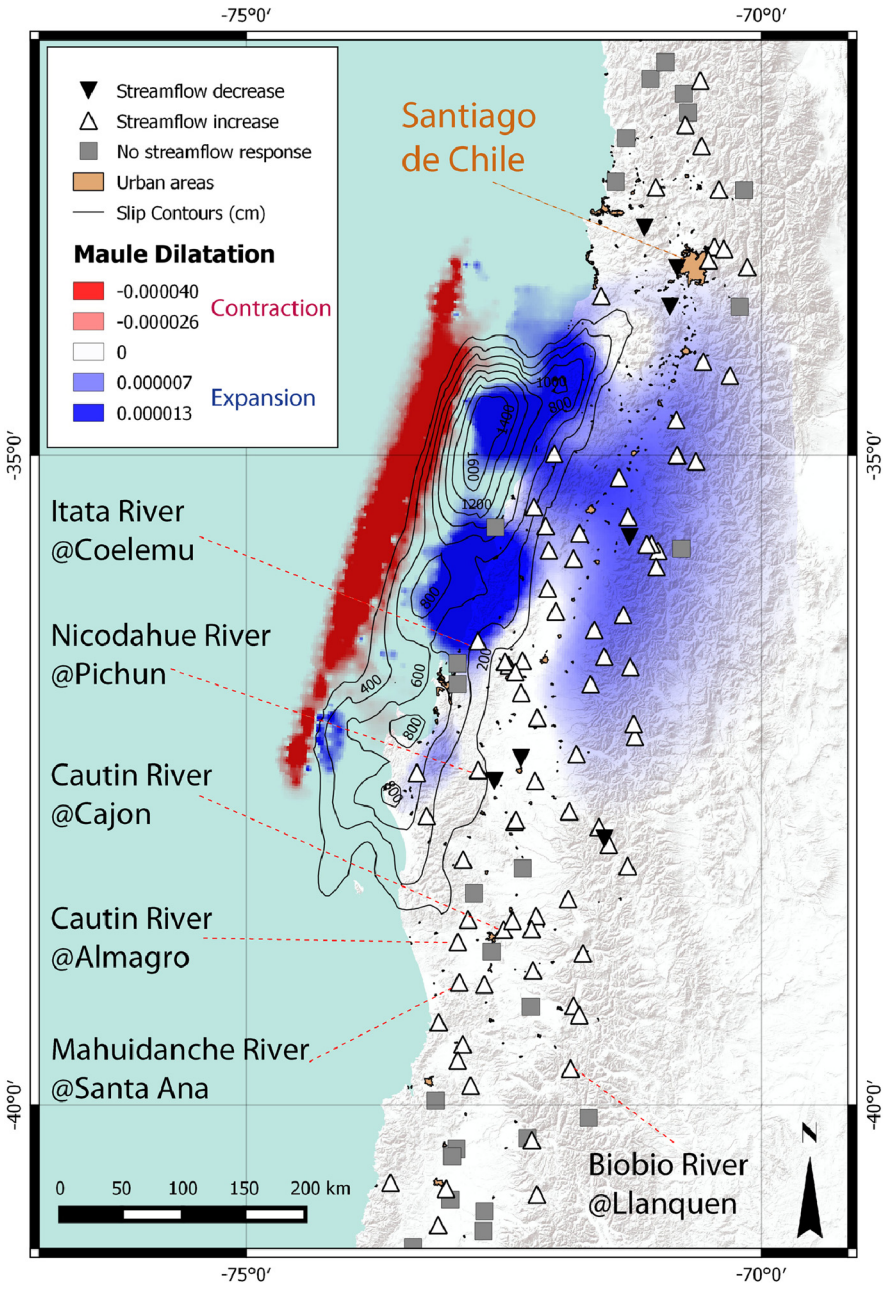

Fig. 4. Regional streamflow responses. Regional pattern of post-seismic streamflow responses and distribution of static strain, modeled as the relative volume change using Coulomb 3.3 (Lin and Stein, 2004; Toda et al., 2005). The red zones show contraction while the blue zones indicate dilatation. Contour lines show the horizontal slip with intervals of 200 cm (Tong et al., 2010). Base map is Esri World Terrain Base layer (http://services.arcgisonline.com/arcgis/rest/services/World_Terrain_Base/MapServer, accessed 10.07.2016). For highlighted gauging stations refer to Fig. 3. (For interpretation of the references to color in this figure legend, the reader is referred to the web version of this article.)

and

$$\frac{\partial h(0,t)}{\partial x} = 0. \tag{6}$$

At time of the earthquake, $t = 0$, we assume that hydraulic head increases an amount h_0 over a distance $0 < x < U'$. We formalize the initial condition as

$$h(x,0) = h_0 \quad \text{with } 0 < x < U'. \tag{7}$$

Recharge occurs over a distance $0 < x < U'$ The discharge at the time of the earthquake is Q_0.

The last significant rainfall event occurred about ten days before the earthquake, which is long enough to allow the head to reach a stationary evolving distribution. Under this assumption and a constant D, we can extend the co-seismic recharge model (Wang et al., 2004b) by accounting for long-term streamflow recession. The solution is then:

$$Q(t) = Q_0 e^{-\pi^2 Dt/4U^2} + \frac{2DQ_t}{UU'} \sum_{r=1}^{\infty} (-1)^{r-1} \sin\frac{(2r-1)\pi U'}{2U} e^{-\frac{(2r-1)\pi^2 D}{4U^2}t}, \tag{8}$$

where Q_t is total excess water released by the earthquake, and t is the time since the earthquake. We fitted equation (8) using least squares and three parameters U'/U, D/U^2 and Q_t to the

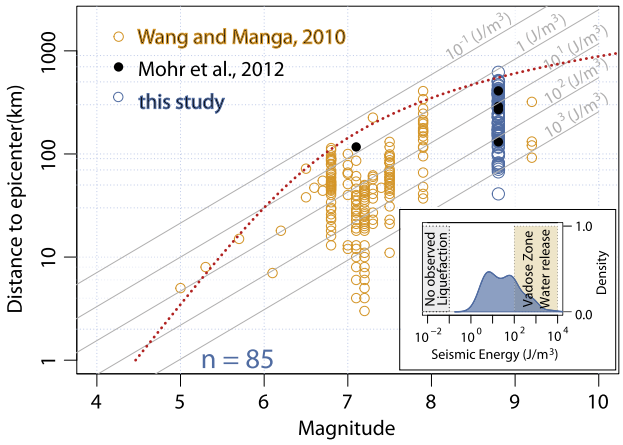

Fig. 5. Earthquake magnitude–distance relationship. Seismically triggered streamflow changes (circles) as a function of earthquake magnitude and distance from epicenter. Orange circles are data from (Wang and Manga, 2010a); black circles are data from the Maule earthquake, and the M7.1 2011 Araucania aftershock in Chilean headwater catchments (Mohr et al., 2012); blue circles are data from this study. Red dashed line is an empirical bound for observed liquefaction (Papadopoulos and Lefkopoulos, 1993). Grey lines are seismic energy density (J/m^3) (Wang and Manga, 2010b). Inset shows the seismic energy density estimated for the studied catchments, and domains for liquefaction (Wang and Manga, 2010b) and release of vadose zone water in nearly saturated sandy soils (Mohr et al., 2015). (For interpretation of the references to color in this figure legend, the reader is referred to the web version of this article.)

streamflow data post-dating the earthquake, and pre-dating any precipitation events.

2.6. Modeling of vadose zone water release

We quantitatively explore the possible effects of seismically mobilized soil water contributing to discharge. Saturated flow may be initiated when suction provided by matric potential is exceeded by the energy density provided by seismic waves (Mohr et al., 2015). This seismic energy density e (J/m^3) describes the maximum seismic energy available to do work on a unit volume of rock or sediment (Wang and Manga, 2010b), and can be estimated by

$$\log_{10} e\ (\mathrm{J/m^3}) = -3.03 \log_{10} r + 1.45M - 4.24 \qquad (9)$$

where M is earthquake magnitude and r is the epicentral distance (km). We assume that seismic energy density can be superimposed as a positive pressure head ($\Psi_{seismic}$) on the matric potential ($\Psi_{seismic}$). Given this assumption, the static threshold of saturation θ dynamically changes during shaking (Van Genuchten, 1980) to:

$$_{(\Psi_{seismic}+\Psi_{matric})} = \left[1 + \left[\alpha * (\Psi_{seismic} + \Psi_{matric})\right]^n\right]^{-1+\frac{1}{n}} \qquad (10)$$

We combine the van Genuchten water-retention model with a Monte Carlo simulation performing 1000 iterations to simulate the amount of water that seismic shaking could have released from soil columns. To this end, we consider empirical texture-specific soil-hydraulic parameters α and n for clayey to sandy soil textures (http://eusoils.jrc.ec.europa.eu/ESDB_Archive/ESDBv2/popup/hy_param.htm), published soil thicknesses for south-central Chile (42–130 cm) (Casanova et al., 2013), the potential range of residual and saturated soil water content (0.01–0.025, and 0.366–0.614, respectively), and the calculated seismic energy densities for each catchment using an empirical relation based on ground motion data in Southern California (Wang, 2007). We refer to Supplement 2 for a map of soil types within the greater study area.

3. Results

At least 85 streams responded to the Maule earthquake, with 78 increasing and seven decreasing their discharge following the seismic shock. At least 137 streams had no obvious changes in streamflow. Responses occurred in the Andes, the Coastal Mountains, and the Central Valley, up to 620 km away from the epicenter (Fig. 3, Fig. 4, Fig. 5). We estimate a total excess discharge of 1.12 ± 0.03 km^3 (Fig. 6a), considering only streams with a clear response. Where larger catchments contained smaller ones with seismic streamflow responses, we included only the trunk catchment for calculating excess discharge. Scaled to catchment area, excess water ranged between 3 and 56 mm (Fig. 6b, Table 1) with two exceptions: for the Claro River and the Rucue River, we estimated 506 and 844 mm, respectively. We ran an additional recession analysis of excess water to check for dam breaks that could have caused this massive increase. To this end we followed the steps for the recession analysis (section 2.3) and compared the recession constants for single rainfall–runoff events before the earthquake with the excess water wave immediately after the earthquake. While this analysis shows a slight post-seismic increase for the Claro catchment, we find a decrease for the Rucue River, with slower recession compared to rainfall–runoff recessions before the earthquake, so that we can exclude a dam break for this river.

The random forest classifier performed well with an out-of-bag error rate of 10.4%. Of the 85 streams showing responses, seven were misclassified as non-responding, whereas 16 out of 137 stations with no observed response were misclassified as responsive. Earthquake attributes such as distance from the epicenter, and mean and maximum PGV and PGA, were among the most important predictors of observed streamflow response (Fig. 7). Among the topographic predictors, only the skewness of elevation, a measure of topographic extremes, notably affected the classification.

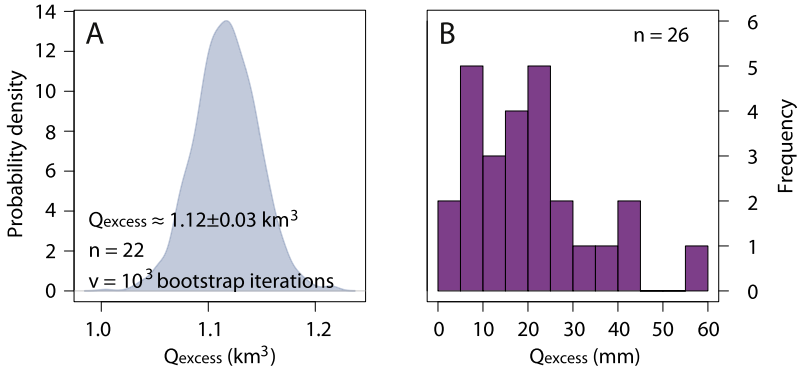

Fig. 6. Excess discharge. Estimates of seismically generated excess discharge in Chilean rivers following the 2010 Maule earthquake. A: Probability density of estimated total excess water (km^3) for 22 modeled catchments based on 1000 bootstrapped iterations (Table 1). Uncertainty is given as $\pm 1\sigma$, bandwidth is 0.00687. B: Histogram of the observed excess water scaled to catchment area (mm). *Note*: 26 catchments were modeled, though 22 were considered for excess discharge quantifications owing to 4 catchments draining into larger ones.

Please cite this article in press as: Mohr, C.H., et al. Regional changes in streamflow after a megathrust earthquake. Earth Planet. Sci. Lett. (2016), http://dx.doi.org/10.1016/j.epsl.2016.11.013

Table 1
Modeled excess discharge for the catchments and model parameters. Error bars are $\pm 1\sigma$.

Stream	Q_0 ($\times 10^6$ m^3)	Area ($\times 10^4$ km^2)	Q_0 (mm)	U'/U	D/U^2 (day^{-1})
Rio Maule @ Forel	141 ± 25	2.0759	6.8	0.7	0.0179 ± 0.0047
Rio Maipo @ Cabinbao	84.4 ± 9.1	1.4657	5.6	0.9	0.0058 ± 0.0007
Rio Itata @ Coelemu	163 ± 5	1.0218	16.0	0.7	0.0288 ± 0.0011
Rio Loncomilla @ las Brisas	62 ± 6.8	1.0190	6.1	0.7	0.0174 ± 0.0027
Rio Loncomillo @ Bodega	22.7 ± 1.6	0.7298	3.1	0.5	0.038 ± 0.0038
Rio Mataquito @ Licanten	117 ± 5	0.5720	20.4	0.7	0.0133 ± 0.0008
Rio Aconcagua @ Romeral	15.6 ± 7	0.5579	2.8	0.3	0.0596 ± 0.0033
Rio Cautin @ Almagro	83.9 ± 3.8	0.5543	15.1	0.8	0.0055 ± 0.0003
Rio Cholchol @ Cholchol	68 ± 1.5	0.5039	13.5	0.7	0.0054 ± 0.0002
Rio Itata @ Balsa Nueva	26.5 ± 4.4	0.4498	5.6	0.8	0.0126 ± 0.0035
Rio Bio Bio @ LLanquen	40 ± 1.2	0.3369	12.3	0.7	0.0067 ± 0.0003
Rio Cautin @ Cajon	62.8 ± 1.9	0.2703	23.2	0.8	0.0031 ± 0.0001
Rio Melado @ Salto	86.4 ± 5.5	0.2137	40.5	0.8	0.0119 ± 0.0012
Rio Allipen @ Los Laureles	92.9 ± 3.7	0.1672	55.6	0.9	0.0017 ± 0.0001
Rio Uble @ Forel	34 ± 0.4	0.1651	20.6	0.8	0.0036 ± 0.0001
Rio Perquilauguen @ Gniquen	8.4 ± 0.9	0.1295	6.5	0.8	0.1129 ± 0.0231
Rio Polcura	15.9 ± 0.7	0.0909	4.7	0.8	0.0048 ± 0.0002
Rio Putaendo @ Resguardo Los Patos	9.8 ± 0.2	0.0889	11.0	0.8	0.0023 ± 0.0001
Rio Lumaco @ Lumaco	20.3 ± 0.6	0.0856	23.7	0.8	0.0033 ± 0.0001
Rio Allipen @ Melipeuco	35.1 ± 0.6	0.0821	42.7	0.9	0.0017 ± 0
Rio Nicodahue	21.5 ± 0.9	0.0740	29.1	0.7	0.0074 ± 0.0004
Rio Claro @ Camarico	328 ± 44	0.0648	506.3	0.8	0.0093 ± 0.0016
Rio Sauces	16.7 ± 0.9	0.0599	27.9	0.8	0.0031 ± 0.0002
Rio Longavi @ El Castillo	14.9 ± 0.3	0.0467	31.9	0.8	0.0041 ± 0.0001
Rio Mahuidanche @ Santa Ana	7.5 ± 0.3	0.0383	19.6	0.8	0.0048 ± 0.0003
Rio Purapel @ Nirivilo	6.1 ± 0.2	0.0263	23.2	0.8	0.0041 ± 0.0003
Rio Rucue @ Camino	178 ± 6	0.0211	843.3	0.9	0.001 ± 0
Rio Las Leas @ Rio Cachpoal	6.1 ± 0.5	0.0174	35.1	0.7	0.0067 ± 0.0004

Positive skewness reflects a high percentage of low-lying areas, whereas negative skewness indicates that higher-lying areas dominate. Surprisingly, geology and tectonic features were among the less important predictors. The same applies to rainfall and land cover, except for some slight effects of forest cover and partly degraded shrub-lands that are prolific in many catchments (Schulz et al., 2011).

4. Discussion

4.1. Volume of excess water

The estimated excess water released by the Maule earthquake exceeds previously published estimates such as ~0.7 km^3 for the Chi-Chi (Wang et al., 2004a), 0.01 km^3 for the Loma Prieta (Rojstaczer et al., 1995), 0.3 km^3 for the Borah Peak, and 0.5 km^3 for the Hebgen Lake (Muir-Wood and King, 1993) earthquakes, even if leaving out the high excess water yields that we modeled for the Claro and Rucue Rivers (Table 1). Hence, we treat our estimates as a minimum value. This volume of earthquake-released water is particularly relevant as the Maule earthquake occurred towards the end of the dry season, when groundwater resources are depleted. The different amount of excess water released by the Loma Prieta earthquake in California and that released by the Chi-Chi earthquake in Taiwan may reflect the different amounts of rainfall at both sites (Manga, 2001; Wang et al., 2004a). We thus speculate that if the Maule earthquake had struck Chile during wetter periods with higher groundwater levels, we would have expected even higher excess discharge.

For some catchments, the estimated excess water reached monthly discharge yields, such as the Mataquito River whose excess discharge equals roughly the average streamflow for the period between January and February (~19 mm). The Purapel River released excess discharge roughly matching the average discharge during the entire dry season from October to March (~21 mm). This is particularly important for the northern-most responding catchments (e.g., Putaendo River), when compared against annual groundwater recharge rates of <10 mm/yr (Fig. 8). Thus, our minimum excess water estimates highlight the importance of seismo-hydrological recharge in the regional water cycle on at least monthly to seasonal time scales.

We now use our observations to explore possible mechanisms that might have caused the observed streamflow anomalies.

4.2. Did streamflow respond to static strain?

Fig. 4 shows the regional pattern of the streamflow responses with respect to either volumetric expansion or contraction. In contrast to studies documenting a pattern of water-level changes that mimic the distribution of volumetric strain (e.g., Jonsson et al., 2003), streamflow response in our study was uncorrelated with the sign of volumetric strain (see also Supplement 3). Our random forest model also does not reveal any impact of static strain on the sign of streamflow change. Instead, flow increased mainly in areas that experienced expansion, which is in line with many previous studies such as those after the Wechuan and Lushan earthquakes, China (Shi et al., 2014). Our data do not support the idea that volumetric strain dominates regional streamflow responses.

4.3. Did streamflow respond to dynamic strain?

Seismic energy can be estimated empirically as a function of epicentral distance and earthquake magnitude. Wang and Manga (2010b) proposed a minimum of ~0.1 J/m^3 of seismic energy to initiate streamflow responses. With this bound, the Maule earthquake would have generated sufficient energy to cause responses in all catchments (Fig. 5). We find that nearly all catchments are within an empirical threshold for liquefaction as a function of epicentral distance and earthquake magnitude (Papadopoulos and Lefkopoulos, 1993). In general, consolidation up to liquefaction may be theoretically possible (Montgomery and Manga, 2003). However, the responses occurred within the headwater catchments of the Andes and the Coastal Mountains where reported liquefaction features were rare. The liquefaction hypothesis favors stream-

Please cite this article in press as: Mohr, C.H., et al. Regional changes in streamflow after a megathrust earthquake. Earth Planet. Sci. Lett. (2016), http://dx.doi.org/10.1016/j.epsl.2016.11.013

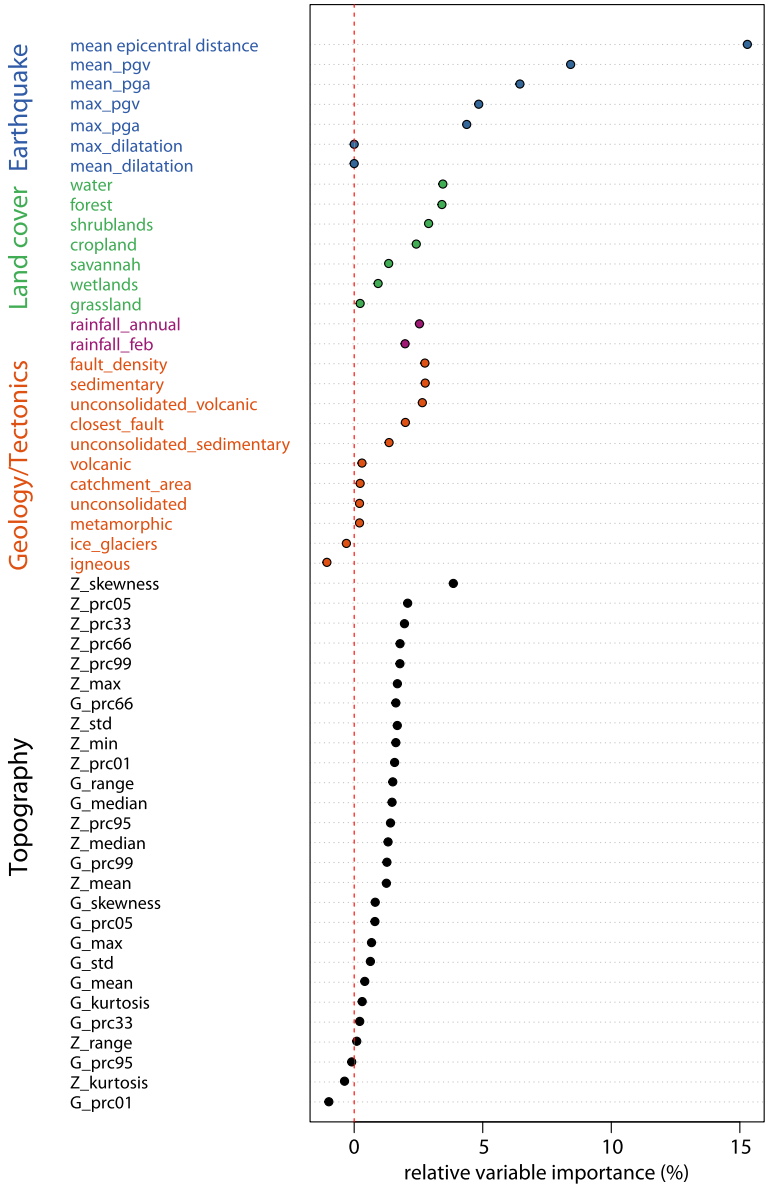

Fig. 7. Random forest variable importance. Relative variable importance for a random forest classifier of earthquake-triggered stream response. All predictor variable importance was normalized to 100%. See Supplement 1 for a full description of the predictors. *Note*: "Unconsolidated_sedimentary and "unconsolidated" refers to the limited possibility to unambiguously transfer Spanish geological vocabulary into English geological terms.

flow response on saturated floodplains at low elevations instead (Cox et al., 2012; Montgomery et al., 2003), and is thus inconsistent with our observations (Fig. 4). Moreover, the presence of unconsolidated material is not required to explain the altered discharges after the Maule earthquake (Fig. 7). Mohr et al. (2012) showed that undrained consolidation of the deep (~5–6 m) saturated saprolite may have played a role in small catchments of the Coastal Mountains, though we cannot assume that a deeply weathered saprolite prone to liquefaction underlies all affected catchments (Casanova et al., 2013). Thus, we discard undrained consolidation as a dominant process at the regional scale.

4.4. Did streamflow respond to water released from the vadose zone?

Assuming water contents close to saturation in sandy soils, and sufficient connectivity between saturated and unsaturated zones, seismic energy density can dynamically lower the soil matric potential, which in turn releases soil water to groundwater (Mohr et al., 2015). Yet, only some catchments were shaken with an intensity that has been found to be theoretically sufficient to release vadose zone water (Fig. 5). The Maule earthquake occurred near the end of the dry season, so that we assume that soils were dry, restricting the soil column close to saturation, and thus prone for water losses, to less than half of the total soil depth. We obtained a median excess water of <9 mm, which is well below the modeled excess water (Fig. 6b), so that the release of soil water is insufficient to explain the streamflow response as a whole. Even if it were, some connectivity between the unsaturated and saturated zone is required during shaking. Earthquakes cause transient stresses from waves that can establish connectivity via clearing clogged pores (Candela et al., 2014). In the absence of well data, we estimate the average groundwater table to first order at 57 ± 24 m below the surface for all catchments, based on model data (Fan et al., 2013). Following Montgomery et al. (2003), our Monte Carlo simulation yields streamflow response times of $\sim 3 \pm 3$ h, assuming maximum distances of 57 ± 24 m

Please cite this article in press as: Mohr, C.H., et al. Regional changes in streamflow after a megathrust earthquake. Earth Planet. Sci. Lett. (2016), http://dx.doi.org/10.1016/j.epsl.2016.11.013

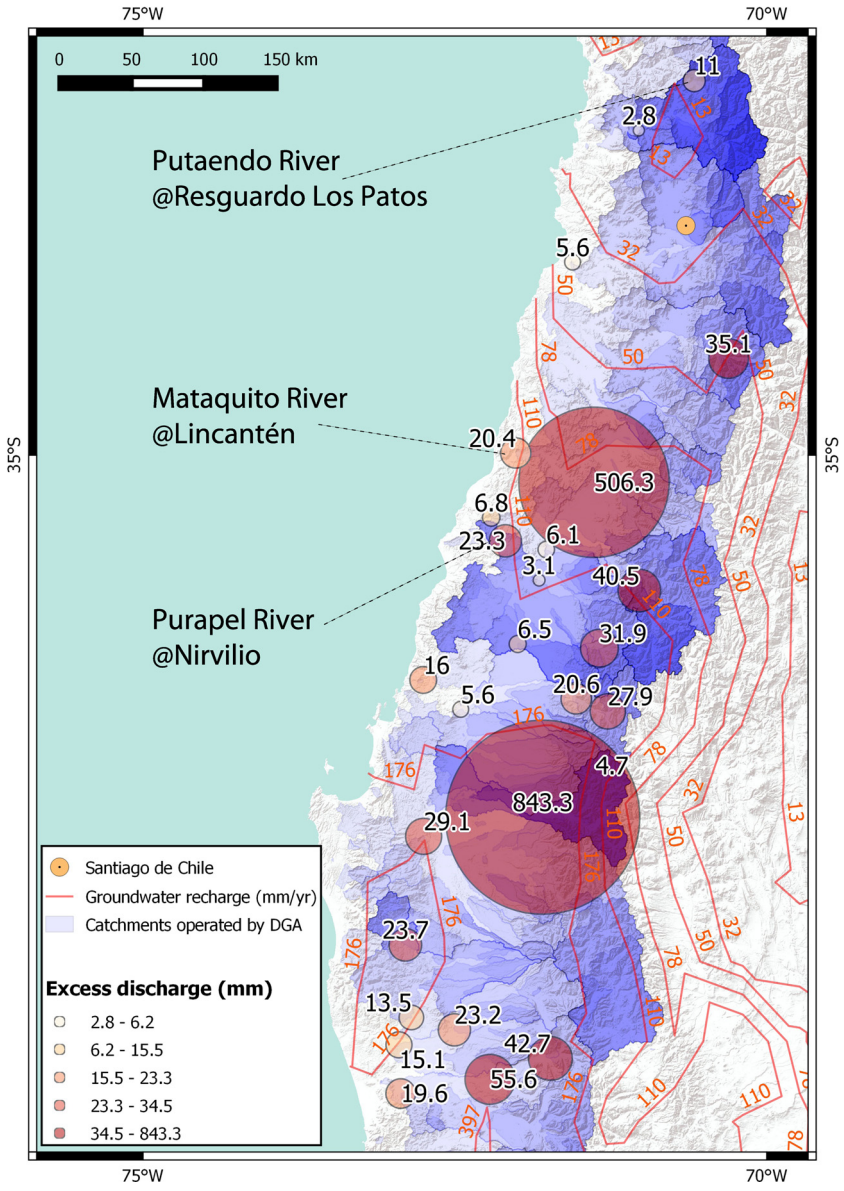

Fig. 8. Groundwater recharge and excess discharge. Excess discharge vs modeled groundwater recharge rates for south-central Chile. Orange contour lines show 10th quantiles of modeled groundwater recharge rates (Hannes Müller Schmied, 2016, personal data). Orange colored numbers show groundwater recharge rate in mm/yr. Groundwater recharge is modeled using the Global Hydrology and Water Use Model WaterGAP at a spatial resolution of 0.5° × 0.5° geographical latitude and longitude, respectively (Müller Schmied et al., 2014). Excess discharge is scaled by color and circle size. Black numbers show estimated excess water in mm. Base map is Esri World Terrain Base layer (http://services.arcgisonline.com/arcgis/rest/services/World_Terrain_Base/MapServer, accessed 20.07.2016). For highlighted gauging stations refer to text in section 4.1. (For interpretation of the references to color in this figure legend, the reader is referred to the web version of this article.)

from the source of excess water for the streamflow discharge feeding aquifers, and typical hydraulic diffusivities for unconsolidated sands of 10^0–10^1 m^2/s (Roeloffs, 1996). We considered such relatively high diffusivities because we cannot assume that the near-surface geology remains undamaged in areas of high seismicity (e.g., Scott et al., 2016) which in turn would increase permeability (Wang et al., 2004a). These response times correspond very closely with streamflow responses observed in instrumented headwater catchments after the Maule earthquake (Mohr et al., 2012). Response times of hours are plausible for groundwater conditions (Wang and Manga, 2010a), but differ from the time scale of shaking (~2.5 min) during which the released soil water has to reach the underlying aquifer from the vadose zone. We argue that the groundwater table is too deep to be recharged by mobilized soil water during seismic shaking, and discard the mechanism of soil-water release for explaining the regional streamflow responses.

4.5. Did streamflow respond to enhanced permeability?

Groundwater flow is dominated by the highest permeability layer within a hydrological system. Thus, recession analysis can only reveal changes in near-surface permeability assuming isotropic conditions (Wang and Manga, 2010a). In that case, our recession analysis does not support post-seismic changes in lateral hydraulic conductivity (Fig. 9), so that we exclude enhanced lateral permeability as documented in wells (Elkhoury et al., 2006), as a cause of the streamflow anomalies. This inference is consistent with previous recession analyses for headwater catchments in south-central Chile (Mohr et al., 2012). Instead, our results are consistent with enhanced vertical permeability, for example by breaching impervious geological layers via subvertical tension cracks (Wang et al., 2016) or clearing clogged pore throats (Candela et al., 2014), allowing the groundwater to drain vertically without affecting base-flow recession. This model leads to

Please cite this article in press as: Mohr, C.H., et al. Regional changes in streamflow after a megathrust earthquake. Earth Planet. Sci. Lett. (2016), http://dx.doi.org/10.1016/j.epsl.2016.11.013

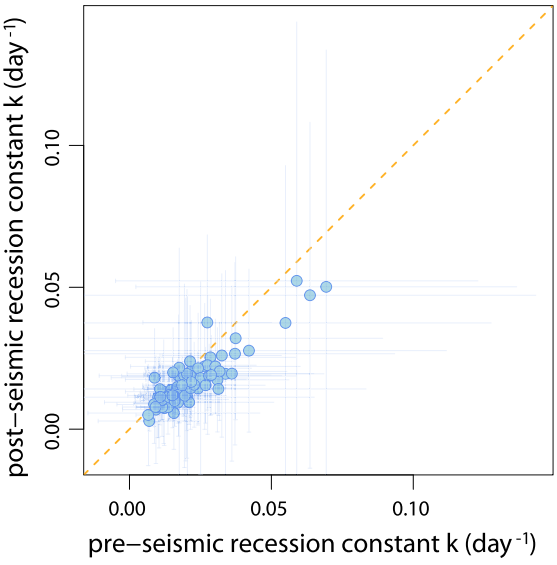

Fig. 9. Recession constants. Pre- versus post-seismic recession constants of estimated base flow (Nathan and McMahon, 1990), calculated as daily values (m^3/day) over one year each for catchments with observed streamflow response. Error bars are $\pm 1\sigma$ of daily recession constants.

enhanced discharge by elevating the hydraulic head following the release of additional water from higher areas (Wang et al., 2004a). The model predicts groundwater recharge in elevated areas and discharge at hillslope toes. This general pattern is consistent with the results from the random forest classification, in which topographic extremes have some importance (Fig. 7). Hence, both approaches, i.e., the physics-based modeling and the machine learning algorithm, support the enhanced vertical permeability mechanism. However, small upland catchments are not exclusively areas of discharge (Tóth, 1963) as predicted by our model. Instead, recharge may also take place in such settings. Thus, we do not necessarily expect that post-seismic increases and decreases are limited to lower and higher elevations, respectively (Fig. 4). The model with water added coseismically captures the time evolution of the excess discharge as observed across the Andes and Coastal Mountain Range Mountains and the Central Valley (Fig. 3), hence supporting the general validity of the model. Taken together, our data suggest that enhanced vertical permeability most plausibly explains the regional streamflow response to the Maule earthquake, with discharge increasing mostly across the Andes and the Coastal Mountains.

5. Conclusions

We present new evidence for widespread earthquake-driven discharge changes in several dozen Andean and Coastal Range catchments characterized by steep hydro-climatic, groundwater and topographic gradients. We report the largest reported volume of water ever released (>1.12 km^3) by an earthquake, and combine physics-based modeling with statistical analyses to argue for a seismically induced increase in vertical permeability as the most plausible mechanism for explaining the regional hydrological responses to the 2010 Maule earthquake. We cannot, however, provide independent evidence for that mechanism and further testing of the model is required. Compared to groundwater recharge rates as low as 10–20 mm/yr for the northern-most affected catchments, the massive discharge of excess water is similar to seasonal discharge; assuming a mean recurrence interval of ~25 yr for >M8 earthquakes, our study emphasizes the substantial impact of earthquakes on groundwater resources in Chile's arid catchments in particular.

Acknowledgements

We appreciate the financial support by the Potsdam Graduate School awarded to C.H.M. and NSF grant EAR1344424 to M.M. and C.Y.W. Jan Seidemann, Jenny Tamm, Johannes Schnell, Marta Enesco and Laura Giese helped with GIS and data analyses. We also thank Hannes Müller Schmied and Petra Döll, University of Frankfurt, Germany, for sharing modeled groundwater recharge data, and Wolfgang Schwanghart for helping with the Topo Toolbox. We value the constructive comments by Peter Shearer and two anonymous reviewers. We used the R programming environment with packages Tiger (D. Reusser, Tiger: Time Series of Grouped Errors, unpublished data, 2010, http://cran.r-project.org/web/packages/tiger), EcohydRology (D.R. Fuka, M.T. Walter, J.A. Archibald, T.S. Steenhuis and Z.M. Easton, 2014, https://cran.r-project.org/web/packages/EcoHydRology/index.html) and randomForest (Liaw and Wiener, 2015, https://cran.r-project.org/web/packages/randomForest).

Appendix A. Supplementary material

Supplementary material related to this article can be found online at http://dx.doi.org/10.1016/j.epsl.2016.11.013.

References

Beresnev, I.A., Johnson, P.A., 1994. Elastic-wave stimulation of oil production – a review of methods and results. Geophysics 59, 1000–1017.

Beven, K., 1995. Linking parameters across scales: subgrid parameterizations and scale dependent hydrological models. Hydrol. Process. 9 (5–6), 507–525. http://dx.doi.org/10.1002/hyp.3360090504.

Blume, T., Zehe, E., Bronstert, A., 2007. Rainfall–runoff response, event-based runoff coefficients and hydrograph separation. Hydrol. Sci. J. 52, 843–862. http://dx.doi.org/10.1623/hysj.52.5.843.

Breiman, L., 2001. Random forests. Mach. Learn. 45, 5–32. http://dx.doi.org/10.1023/A:1010933404324.

Candela, T., Brodsky, E.E., Marone, C., Elsworth, D., 2014. Laboratory evidence for particle mobilization as a mechanism for permeability enhancement via dynamic stressing. Earth Planet. Sci. Lett. 392, 279–291. http://dx.doi.org/10.1016/j.epsl.2014.02.025.

Carrigan, C.R., King, G.C.P., Barr, G.E., Bixler, N.E., 1991. Potential for water-table excursions induced by seismic events at Yucca Mountain, Nevada. Geology 19, 1157–1160. http://dx.doi.org/10.1130/0091-7613(1991)019<1157:PFWTEI>2.3.CO;2.

Casanova, M., Salazar, O., Seguel, O., Luzio, W., 2013. The Soils of Chile. Springer, Dordrecht.

Channan, S., Collins, K., Emanuel, W.R., 2014. Global Mosaics of the Standard MODIS Land Cover Type Data. University of Maryland and the Pacific Northwest National Laboratory, College Park, MD, USA.

Charmoille, A., Fabbri, O., Mudry, J., Guglielmi, Y., Bertrand, C., 2005. Post-seismic permeability change in a shallow fractured aquifer following a M_L 5.1 earthquake (Fourbanne karst aquifer, Jura outermost thrust unit, eastern France). Geophys. Res. Lett. 32, L18406. http://dx.doi.org/10.1029/2005GL023859.

Chen, J.S., Wang, C.Y., 2009. Rising springs along the Silk Road. Geology 37, 243–246. http://dx.doi.org/10.1130/G25472A.1.

Cox, S.C., Rutter, H.K., Sims, A., Manga, M., Weir, J.J., Ezzy, T., White, P.A., Horton, T.W., Scott, D., 2012. Hydrological effects of the M_W 7.1 Darfield (Canterbury) earthquake, 4 September 2010, New Zealand. N.Z. J. Geol. Geophys. 55, 231–247. http://dx.doi.org/10.1080/00288306.2012.680474.

Elkhoury, J.E., Brodsky, E.E., Agnew, D.C., 2006. Seismic waves increase permeability. Nature 441, 1135–1138. http://dx.doi.org/10.1038/nature04798.

Fan, Y., Li, H., Miguez-Macho, G., 2013. Global patterns of groundwater table depth. Science 339, 940–943. http://dx.doi.org/10.1126/science.1229881.

Fleeger, G.M., Goode, D.J., 1999. Hydrologic Effects of the Pymatuning Earthquake of September 25, 1999, in Northwestern Pennsylvania. USGS WRIR 99-4170.

Friedl, M.A., Sulla-Menashe, D., Tan, B., Schneider, A., Ramankutty, N., Sibley, A., Huang, X., 2010. MODIS Collection 5 Global Land Cover: Algorithm Refinements and Characterization of New Datasets, Collection 5.1 IGBP Land Cover. Boston University, Boston, MA, USA.

Galassi, D.M.P., Lombardo, P., Fiasca, B., Di Cioccio, A., Di Lorenzo, T., Petitta, M., Di Carlo, P., 2014. Earthquakes trigger the loss of groundwater biodiversity. Sci. Rep. 4. http://dx.doi.org/10.1038/srep06273.

Guérin, A., Devauchelle, O., Lajeunesse, E., 2014. Response of a laboratory aquifer to rainfall. J. Fluid Mech. 759. http://dx.doi.org/10.1017/jfm.2014.590.

Hastie, T., Tibshirani, R., Freidman, J., 2009. The Elements of Statistical Learning – Data Mining, Inference, and Prediction. Springer, New York.

Hijmans, R.J., Cameron, S.E., Parra, J.L., Jones, P.G., Jarvis, A., 2005. Very high resolution interpolated climate surfaces for global land areas. Int. J. Climatol. 25, 1965–1978. http://dx.doi.org/10.1002/joc.1276.

Jarvis, A., Reuter, H.I., Nelson, A., Guevara, E., 2008. Hole-filled SRTM for the globe version 4. Available from the CGIAR-CSI SRTM 90 m database http://srtm.csi.cgiar.org.

Jonsson, S., Segall, P., Pedersen, R., Bjornsson, G., 2003. Post-earthquake ground movements correlated to pore–pressure transients. Nature 424, 179–183. http://dx.doi.org/10.1038/nature01776.

Kampf, S., Burges, S., 2007. A framework for classifying and comparing distributed hillslope and catchment hydrologic models. Water Resour. Res. 43 (5). http://dx.doi.org/10.1029/2006WR005370.

Liaw, A., Wiener, M., 2002. Classification and regression by randomForest. R News 2, 18–22.

Lin, J., Stein, R.S., 2004. Stress triggering in thrust and subduction earthquakes, and stress interaction between the southern San Andreas and nearby thrust and strike-slip faults. J. Geophys. Res. 109. http://dx.doi.org/10.1029/2003JB002607.

Manga, M., 2001. Origin of postseismic streamflow changes inferred from baseflow recession and magnitude–distance relations. Geophys. Res. Lett. 28, 2133–2136. http://dx.doi.org/10.1029/2000GL012481.

Manga, M., Beresnev, I., Brodsky, E.E., Elkhoury, J.E., Elsworth, D., Ingebritsen, S.E., Mays, D.C., Wang, C.Y., 2012. Changes in permeability caused by transient stresses: field observations, experiments, and mechanisms. Rev. Geophys. 50. http://dx.doi.org/10.1029/2011RG000382.

Manga, M., Rowland, J.C., 2009. Response of Alum Rock springs to the October 30, 2007 Alum Rock earthquake and implications for the origin of increased discharge after earthquakes. Geofluids 9, 237–250. http://dx.doi.org/10.1111/j.1468-8123.2009.00250.x.

Manga, M., Wang, C.Y., 2015. 4.12. Earthquake hydrology. In: Schubert, G. (Ed.), Treatise on Geophysics, second edition. Elsevier, Oxford, pp. 305–328.

Mohr, C.H., Manga, M., Wang, C.-y., Kirchner, J.W., Bronstert, A., 2015. Shaking water out of soil. Geology 43, 207–210. http://dx.doi.org/10.1130/G36261.1.

Mohr, C.H., Montgomery, D.R., Huber, A., Bronstert, A., Iroumé, A., 2012. Streamflow response in small upland catchments in the Chilean coastal range to the M_W 8.8 Maule earthquake on 27 February 2010. J. Geophys. Res., Earth Surf. 117. http://dx.doi.org/10.1029/2011JF002138.

Montgomery, D.R., Greenberg, H.M., Smith, D.T., 2003. Streamflow response to the Nisqually earthquake. Earth Planet. Sci. Lett. 209, 19–28. http://dx.doi.org/10.1016/S0012-821X(03)00074-8.

Montgomery, D.R., Manga, M., 2003. Streamflow and water well responses to earthquakes. Science 300, 2047–2049. http://dx.doi.org/10.1126/science.1082980.

Muir-Wood, R., King, G.C.P., 1993. Hydrological signatures of earthquake strain. J. Geophys. Res., Solid Earth 98, 22035–22068. http://dx.doi.org/10.1029/93JB02219.

Müller Schmied, H., Eisner, S., Franz, D., Wattenbach, M., Portmann, F.T., Flörke, M., Döll, P., 2014. Sensitivity of simulated global-scale freshwater fluxes and storages to input data, hydrological model structure, human water use and calibration. Hydrol. Earth Syst. Sci. 18, 3511–3538. http://dx.doi.org/10.5194/hess-18-3511-2014.

Nathan, R.J., McMahon, T.A., 1990. Evaluation of automated techniques for base flow and recession analyses. Water Resour. Res. 26, 1465–1473. http://dx.doi.org/10.1029/WR026i007p01465.

NCEDC, 2014. Northern California Earthquake Data Center. UC Berkeley Seismological Laboratory. Dataset. http://dx.doi.org/10.7932/NCEDC.

Papadopoulos, G.A., Lefkopoulos, G., 1993. Magnitude–distance relations for liquefaction in soil from earthquakes. Bull. Seismol. Soc. Am. 83, 925–938.

Pliny, the Elder, ca. AD 77–79. The Natural History.

Roeloffs, E., 1996. Poroelastic techniques in the study of earthquake-related hydrologic phenomena. Adv. Geophys. 37 (37), 135–195. http://dx.doi.org/10.1016/S0065-2687(08)60270-8.

Rojstaczer, S., Wolf, S., Michel, R., 1995. Permeability enhancement in the shallow crust as a cause of earthquake-induced hydrological changes. Nature 373, 237–239. http://dx.doi.org/10.1038/373237a0.

Schulz, J.J., Cayuela, L., Rey-Benayas, J.M., Schröder, B., 2011. Factors influencing vegetation cover change in Mediterranean Central Chile (1975–2008). Appl. Veg. Sci. 14, 571–582. http://dx.doi.org/10.1111/j.1654-109X.2011.01135.x.

Schwanghart, W., Scherler, D., 2014. Short communication: TopoToolbox 2 – MATLAB-based software for topographic analysis and modeling in Earth surface sciences. Earth Surf. Dyn. 2, 1–7. http://dx.doi.org/10.5194/esurf-2-1-2014.

Scott, C.P., Allmendinger, R.W., Gonzalez, G., Loveless, J.P., 2016. Coseismic extension from surface cracks reopened by the 2014 Pisagua, northern Chile, earthquake sequence. Geology 44 (5), 387–390. http://dx.doi.org/10.1130/g37662.1.

SERNAGEOMIN, 2003. Mapa Geologico de Chile: Version Digital, Publicación Geológica Digital, No. 4, Servicio Nacional de Geología y Minería, Santiago de Chile (CD-ROM, versión 1.0, 2003).

Sexton, J.O., Song, X.-P., Feng, M., Noojipady, P., Anand, A., Huang, C., Kim, D.-H., Collins, K.M., Channan, S., DiMiceli, C., Townshend, J.R., 2013. Global, 30-m resolution continuous fields of tree cover: Landsat-based rescaling of MODIS vegetation continuous fields with lidar-based estimates of error. Int. J. Digit. Earth 6, 427–448. http://dx.doi.org/10.1080/17538947.2013.786146.

Shi, Z., Wang, G., Wang, C.-y., Manga, M., Liu, C., 2014. Comparison of hydrological responses to the Wenchuan and Lushan earthquakes. Earth Planet. Sci. Lett. 391, 193–200. http://dx.doi.org/10.1016/j.epsl.2014.01.048.

Strobl, C., Boulesteix, A.L., Kneib, T., Augustin, T., Zeileis, A., 2008. Conditional variable importance for random forests. BMC Bioinform. 9. http://dx.doi.org/10.1186/1471-2105-9-307.

Toda, S., Stein, R.S., Richards-Dinger, K., Bozkurt, S.B., 2005. Forecasting the evolution of seismicity in southern California: animations built on earthquake stress transfer. J. Geophys. Res., Solid Earth 110, B05S16. http://dx.doi.org/10.1029/2004JB003415.

Tong, X.P., Sandwell, D., Luttrell, K., Brooks, B., Bevis, M., Shimada, M., Foster, J., Smalley, R., Parra, H., Soto, J.C.B., Blanco, M., Kendrick, E., Genrich, J., Caccamise, D.J., 2010. The 2010 Maule, Chile earthquake: downdip rupture limit revealed by space geodesy. Geophys. Res. Lett. 37. http://dx.doi.org/10.1029/2010GL045805.

Tóth, J., 1963. A theoretical analysis of groundwater flow in small drainage basins. J. Geophys. Res. 68, 4795–4812. http://dx.doi.org/10.1029/JZ068i016p04795.

Van Genuchten, M.T., 1980. A closed-form equation for predicting the hydraulic conductivity of unsaturated soils. Soil Sci. Soc. Am. J. 44, 892–898.

Wang, C.Y., 2007. Liquefaction beyond the near field. Seismol. Res. Lett. 78 (5). http://dx.doi.org/10.1785/gssrl.78.5.512.

Wang, C.Y., Manga, M., 2010a. Earthquakes and Water. Springer, Berlin, Heidelberg.

Wang, C.Y., Manga, M., 2010b. Hydrologic responses to earthquakes and a general metric. Geofluids 10, 206–216. http://dx.doi.org/10.1002/9781444394900.ch14.

Wang, C.-Y., Manga, M., 2015. New streams and springs after the 2014 Mw6.0 South Napa earthquake. Nat. Commun. 6. http://dx.doi.org/10.1038/ncomms8597.

Wang, C.Y., Wang, C.H., Manga, M., 2004a. Coseismic release of water from mountains: evidence from the 1999 (M_w = 7.5) Chi-Chi, Taiwan, earthquake. Geology 32, 769–772. http://dx.doi.org/10.1130/G20753.1.

Wang, C.Y., Wang, C.H., Kuo, C.H., 2004b. Temporal change in groundwater level following the 1999 (Mw = 7.5) Chi-Chi earthquake, Taiwan. Geofluids 4 (3), 210–220. http://dx.doi.org/10.1111/j.1468-8123.2004.00082.x.

Wang, C.-Y., Manga, M., Wang, C.-H., Chen, C.-H., 2012. Transient change in groundwater temperature after earthquakes. Geology 40, 119–122. http://dx.doi.org/10.1130/G32565.1.

Wang, C.-Y., Liao, X., Wang, L.-P., Wang, C.-H., Manga, M., 2016. Large earthquakes create vertical permeability by breaching aquitards. Water Res. 52. http://dx.doi.org/10.1002/2016WR018893.

Zorner, R.J., Trabucco, A., Bossio, D.A., Verchot, L.V., 2008. Climate change mitigation: a spatial analysis of global land suitability for clean development mechanism afforestation and reforestation. Agric. Ecosyst. Environ. 126, 67–80. http://dx.doi.org/10.1016/j.agee.2008.01.014.

Please cite this article in press as: Mohr, C.H., et al. Regional changes in streamflow after a megathrust earthquake. Earth Planet. Sci. Lett. (2016), http://dx.doi.org/10.1016/j.epsl.2016.11.013